IOP Publishing Phys. Med. Biol. 65 (2020) 025001 (20pp) https://doi.org/10.1088/1361-6560/ab63b4

Physics in Medicine & Biology

IPEM Institute of Physics and Engineering in Medicine

OPEN ACCESS

PAPER

Experimental time resolution limits of modern SiPMs and TOF-PET detectors exploring different scintillators and Cherenkov emission

Stefan Gundacker[1,2,5], Rosana Martinez Turtos[2], Nicolaus Kratochwil[2,3], Rosalinde Hendrika Pots[2,4], Marco Paganoni[1,2], Paul Lecoq[2] and Etiennette Auffray[2]

[1] UniMIB, Piazza dell'Ateneo Nuovo, 1—20126, Milano, Italy
[2] CERN, Esplanade de Particules 1, 1211 Meyrin, Switzerland
[3] University of Vienna, Universitaetsring 1, 1010 Vienna, Austria
[4] RWTH Aachen, Templergraben 55, 52062 Aachen, Germany
[5] Author to whom any correspondence should be addressed.

E-mail: stefan.gundacker@cern.ch

Keywords: TOF PET, silicon photomultiplier (SiPM), single photon time resolution (SPTR), coincidence time resolution (CTR), Cherenkov emission in BGO for fast timing, 10 ps challenge, scintillation kinetics

RECEIVED
4 June 2019

REVISED
11 December 2019

ACCEPTED FOR PUBLICATION
18 December 2019

PUBLISHED
16 January 2020

Abstract

Solid state photodetectors like silicon photomultipliers (SiPMs) are playing an important role in several fields of medical imaging, life sciences and high energy physics. They are able to sense optical photons with a single photon detection time precision below 100 ps, making them ideal candidates to read the photons generated by fast scintillators in time of flight positron emission tomography (TOF-PET). By implementing novel high-frequency readout electronics, it is possible to perform a completely new evaluation of the best timing performance achievable with state-of-the-art analog-SiPMs and scintillation materials. The intrinsic SiPM single photon time resolution (SPTR) was measured with Ketek, HPK, FBK, SensL and Broadcom devices. Also, the best achieved coincidence time resolution (CTR) for these devices was measured with LSO:Ce:Ca of $2 \times 2 \times 3$ mm^3 and $2 \times 2 \times 20$ mm^3 size crystals. The intrinsic SPTR for all devices ranges between 70 ps and 135 ps FWHM when illuminating the entire 3×3 mm^2 or 4×4 mm^2 area. The obtained CTR with LSO:Ce:Ca of $2 \times 2 \times 3$ mm^3 size ranges between 58 ps and 76 ps FWHM for the SiPMs evaluated. Bismuth Germanate (BGO), read out with state of-the-art NUV-HD SiPMs from FBK, achieved a CTR of 158 $\pm$3 ps and 277 $\pm$3 ps FWHM for $2 \times 2 \times 3$ mm^3 and $2 \times 2 \times 20$ mm^3 crystals, respectively. Other BGO geometries yielded 167 $\pm$ 3 ps FWHM for $3 \times 3 \times 3$ mm^3 and 235 $\pm$ 5 ps FWHM for $3 \times 3 \times 15$ mm^3 also coupled with Meltmount ($n = 1.582$) and wrapped in Teflon. Additionally, the average number of Cherenkov photons produced by BGO in each 511 keV event was measured to be 17 $\pm$ 3 photons. Based on this measurement, we predict the limits of BGO for ultrafast timing in TOF-PET with Monte Carlo simulations. Plastic scintillators (BC422, BC418), BaF_2, GAGG:Ce codoped with Mg and CsI:undoped were also tested for TOF performance. Indeed, BC422 can achieve a CTR of 35 $\pm$ 2 ps FWHM using only Compton interactions in the detector with a maximum deposited energy of 340 keV. BaF_2 with its fast cross-luminescence enables a CTR of 51 $\pm$ 5 ps FWHM when coupled to VUV-HD SiPMs from FBK, with only $\sim$22% photon detection efficiency (PDE). We summarize the measured CTR of the various scintillators and discuss their intrinsic timing performance.

1. Introduction

Time of flight positron emission tomography (TOF-PET) substantially benefits from continually improving the coincidence time resolution (CTR), with the goal of ultimately reaching a CTR of 10 ps full width at half maximum (FWHM) (Lecoq 2017) (https://the10ps-challenge.org). In previous works, we have concluded that there is no physical barrier prohibiting such low CTR values in PET (Gundacker 2014, Gundacker *et al* 2016b). However, solutions have to be found to improve the photostatistics of the scintillation process (higher light yield,

Table 1. Overview of the silicon photomultipliers used in this study. The error-bars of the breakdown voltage are in the range of 0.3 V and for the PDE around 3%.

SiPM producer	SPAD size (μm^2)	SiPM size (mm^2)	Breakdown (V) @ 20 °C	PDE (%) @410 nm	Bias[a] (V)
HPK S13360	50 × 50	3 × 3	51.5	62	62
HPK S14160	50 × 50	3 × 3	38.3	60	48
Ketek PM3325 (WBA0)	25 × 25	3 × 3	24.1	57	36
Ketek PM3350 (WBA0)	50 × 50	3 × 3	25.3	55	37
SensL FJ30035	35 × 35	3 × 3	24.4	54	32
Broadcom AFBR-S4N44C013	30 × 30	4 × 4	27.3	60	38
FBK NUV-HD	40 × 40	4 × 4	27.1	65	38
FBK NUV-HD no resin	40 × 40	4 × 4	28.6	65	39
FBK VUV-HD	40 × 40	4 × 4	33.1	58	43

[a] The SiPM bias values are the maximum operational voltages at which the PDE and the time resolution of these devices give best performance.

shorter rise- and decay times) and the single photon time resolution (SPTR) of the photodetector, e.g. silicon photomultiplier (SiPM). Furthermore a complete assessment of currently available scintillators in terms of their achievable time resolution is still missing. This is important, because the appearance of new photodetectors and readout electronics makes it successively possible to explore known and as yet unknown fast scintillation processes. For example recent studies have shown that using Cherenkov emission in Bismuth Germanate $B_4Ge_3O_{12}$ (BGO) upon 511 keV photo-absorption can deliver CTRs in the range of 200 ps FWHM (Kwon *et al* 2016, Brunner and Schaart 2017, Gundacker *et al* 2019).

This paper will present an evaluation and overview of the best timing performance achieved with state-of-the-art SiPMs and scintillation materials available to date. We will discuss the measured intrinsic SPTR of several different SiPM devices (from several producers) and compare their best achievable CTR performance while testing with reference Lutetium Oxyorthosilicate Lu_2SiO_5:Ce (LSO:Ce) codoped with Ca crystals. An overview of the timing performance of various scintillating materials will be given by means of measured CTR, scintillation kinetics (rise- and decay times) and light yield. In particular, we will test BGO and report an average number of Cherenkov photons produced for each 511 keV gamma interaction. Based on these measurements we will analyze and discuss the timing limits of such Cherenkov radiation in TOF-PET.

2. Materials

In this section, an overview of the SiPMs and scintillation materials utilized for our studies is presented.

2.1. Silicon photomultipliers

In table 1 an overview of the tested silicon photomultipliers (SiPMs) from different producers (HPK, Ketek, SensL, Broadcom and FBK) is given. All SiPMs have very similar single photon avalanche diode (SPAD) sizes and active areas, which makes it possible to compare different performances. Figure 1 shows the measured photon detection efficiency (PDE) for the various SiPMs tested as a function of the SiPM bias voltage, at a wavelength of 410 nm. The PDE was measured as described in Eckert *et al* (2010), Acerbi and Gundacker (2019) with pulsed light emitting diodes, excluding the effects of crosstalk and afterpulsing.

2.2. Scintillators

The different scintillator materials used in this study are summarized in table 2 along with the producer name, peak emission wavelength and refractive index at the peak emission. Most of the crystals had a size of $2 \times 2 \times 3$ mm^3. Table 3 shows the measured scintillation light yield of these materials.

The light output (LO) of the scintillators was measured with $2 \times 2 \times 3$ mm^3 or $3 \times 3 \times 3$ mm^3 crystals using a Hamamatsu R2059 photomultiplier tube (PMT), correcting for the wavelength dependent quantum efficiency of the PMT weighted with the scintillation emission. The crystals for the LO measurements were wrapped in Teflon and coupled to the PMT with viscose optical grease ($n_c = 1.42$) Rhodorsil® 47 V (Rhône-Poulenc), except for the case of CsI:undoped, where we used air-coupling ($n_c = 1$). In previous studies we found that in this configuration the crystal cross-section does not influence significantly the light output (Gundacker *et al* 2016a). The light yield of BaF_2 was measured with a $3 \times 3 \times 3$ mm^3 cube wrapped in Teflon and air-coupled to a Hamamatsu H6610 PMT. Values were measured relative to LYSO:Ce (same size, wrapping, coupling), taking into account the weighted PMT quantum efficiencies for LYSO:Ce and BaF_2. The ILY of the scintillators in table 3 was then derived from correcting the measured light output ($LO_{measured}$) with the LTE obtained by Geant4. The light ray

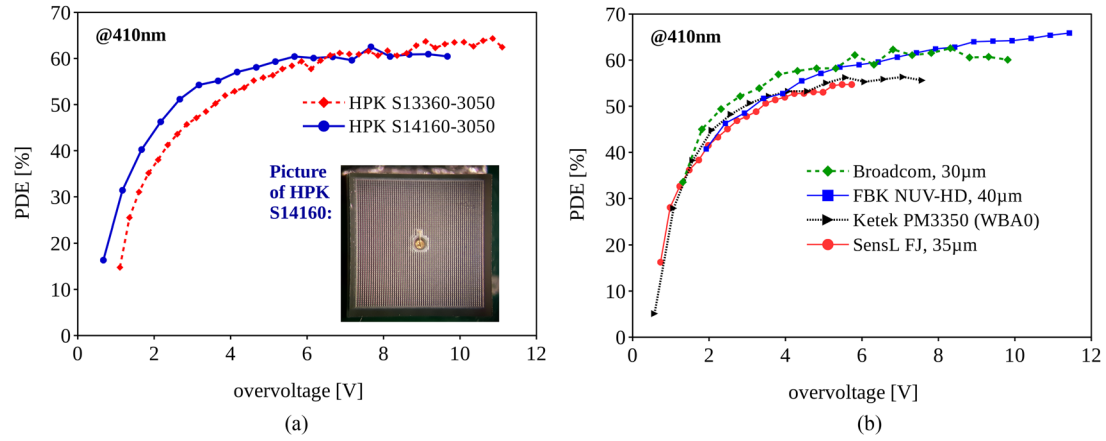

Figure 1. PDE as a function of the SiPM overvoltage measured at 410 nm. (a) Hamamatsu S13360 and S14160 with a photo of HPK S14160 showing the center wire-bond connection, leading to a slight loss of PDE (SPAD pitch is 50 μm). (b) Comparison of the PDE for Broadcom, FBK, Ketek and SensL (now part of ON-semiconductors).

Table 2. Overview of the scintillators used in this work.

Composition	Producer	Emission (nm)	n_{scint} @ emission
LSO:Ce:0.2%Ca	Agile	420	1.82
LSO:Ce:0.4%Ca	Agile	420	1.82
LYSO:Ce	CPI	420	1.82
BGO	SICCAS (China)	480	2.10
BaF_2	Epic-crystals	195/220/310	1.55
CsI:undoped	ISMA (Ukraine)	315	1.95
LuAG:Pr	IPR (Armenia)	320/370	2.03
GAGG:Ce:Mg	C&A	540	1.92
GFAG	C&A	540	1.92
BC418	Saint-Gobain	391	1.58
BC422	Saint-Gobain	370	1.58

Table 3. Overview of the estimated intrinsic light yield (ILY) of the materials used in this work. Light transfer efficiency (LTE) was obtained with Geant4 for a $3 \times 3 \times 3$ mm^3 crystal wrapped in Teflon. The bulk light attenuation and scattering parameters remained constant among the different crystals. The ILY is estimated by considering the refractive-index dependent LTE calculated with Geant4. CsI:undoped and BaF_2 have been measured with air-coupling ($n_c = 1$) due to their UV-emission. ILY errors are in the range of 10%.

Composition	n_{scint} @ emission	LTE @ $n_c = 1$	LTE @ $n_c = 1.42$	$LO_{measured}$ (ph keV^{-1})	ILY (ph keV^{-1})
LSO:Ce:0.2%Ca	1.82	0.46	0.66	—	39.2[a]
LSO:Ce:0.4%Ca	1.82	0.46	0.66	—	32.0[a]
LYSO:Ce	1.82	0.46	0.66	27.1 ($n_c = 1.42$)	41.1
BGO	2.10	0.40	0.58	6.2($n_c = 1.42$)	10.7
BaF_2	1.55	0.53	0.75	—	8.5[b]
CsI:undoped	1.95	0.43	0.62	3.1 ($n_c = 1$)	7.2
LuAG:Pr	2.03	0.41	0.60	—	22.0 [c]
GAGG:Ce:Mg	1.92	0.44	0.63	43.7 ($n_c = 1.42$)	69.4
GFAG	1.92	0.44	0.63	35.1 ($n_c = 1.42$)	55.7
BC418	1.58	0.53	0.74	9.1 ($n_c = 1.42$)	12.3
BC422	1.58	0.53	0.74	7.5 ($n_c = 1.42$)	10.1

[a] Light yield value from Gundacker *et al* (2019).
[b] Measured with HPK PMT H6610 relative to LYSO:Ce (air coupling), corrected for LTE & PDE.
[c] Light yield value from Gundacker *et al* (2016a).

tracing Monte-Carlo simulations include scattering and absorption in the crystal (van der Laan *et al* 2010). A change in refractive index of the material leads to a new total internal refraction of the light rays, hence varying the LTE, shown in table 3. The given LTE values are to be understood as a guidance or approximative, as we do not adapt the surface state, absorption and transmission properties in these simulations for each crystal.

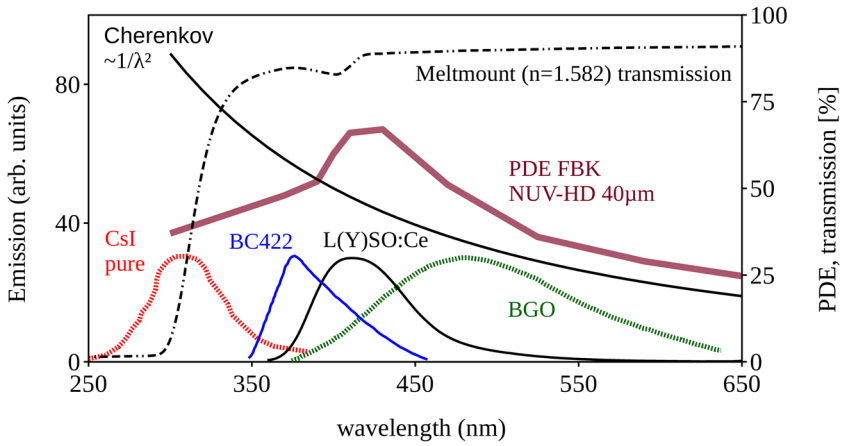

Figure 2. Normalized emission spectra of various scintillators and Cherenkov radiation as compared to the photodetector PDE. The emission spectra of various scintillators and Cherenkov emission are compared with both the UV transmission of the Meltmount coupling compound and the spectral response of a FBK NUV-HD SiPM.

Tables 2 and 3 contain also plastic scintillators, which are of less interest in PET due to their very low density, featuring only Compton scattered events upon 511 keV interaction. However, there are some attempts to use plastic scintillators for certain PET applications (e.g. Compton-PET) because of their otherwise attractiv features, like extremly low-cost, high light yield and fast emission (decay times around 1 ns) (Moskal *et al* 2019). Nevertheless, to understand the limiting factors of the time resolution and the interplay with photostatistics, i.e. scintillation kinetics and light yield, the example of including two plastic scintillators BC418 and BC422 in this test series is very instructive, as will be discussed in more detail later in this work (section 5.3).

In figure 2 we summarize the emission spectra of some scintillators tested, shown together with the transmission behavior of Meltmount ($n = 1.582$). This Meltmount glue was used to couple the scintillators to the FBK NUV-HD SiPMs, to measure the timing performance of the various crystals. Figure 2 further shows the measured PDE of the FBK NUV-HD SiPMs with 40 μm SPAD size. It can be seen that the NUV-HD SiPM is perfectly suited to sense the light from L(Y)SO:Ce(:Ca) scintillators as well as from fast emitting plastic scintillators, like BC422. The PDE even extends to the near ultraviolet making this SiPM suitable to detect Cherenkov emission, for example in BGO (also shown in figure 2). If not stated otherwise all CTR measurements were systematically performed with the crystals wrapped in Teflon (at least three layers) and glued to the SiPMs with Meltmount ($n = 1.582$).

2.3. Cherenkov emission and the 'revival' of BGO

In this work we will have a closer look at BGO and its prominent Cherenkov radiation. Previously BGO was the prefered choice for PET due to its high density, high photofraction and relatively low cost of production. With the application of time of flight in PET, BGO was finally substituted by L(Y)SO:Ce, because of much higher light yield and shorter decay times, assuring good time resolution with PMTs and SiPMs. However, L(Y)SO:Ce is more costly in production and shows intrinsic radioactivity due to the ^{176}Lu decay. Today, emerging ultra-fast SiPMs with adequate PDE in the near ultraviolet (e.g. FBK NUV-HD) make it possible to detect the faint Cherenkov signal produced in BGO upon 511 keV interaction, as shown in figure 2. The basic principle of Cherenkov radiation in TOF-PET applications is the transfer of sufficient energy to an electron in the lattice of the crystal which then exceeds the Cherenkov threshold, i.e. the electron gains enough kinetic energy in order to be faster than the speed of light in the scintillation material (Cherenkov 1934). This can happen upon Compton interactions, transferring part of the 511 keV energy to a quasi free electron, or upon total photo-electric absorption passing the whole 511 keV minus the K-binding shell energy to the freed electron. Cherenkov photons emitted by electrons from Compton scattered events are in principle able to preserve some directionality information of the incomming 511 keV gamma. However, this directionality of the emitted Cherenkov radiation is small, as the electron undergoes several scattering processes in the lattice, changing repeatedly the angle of Cherenkov emission. Photo-electric absorption is by far the most probable event generating Cherenkov photons, which, however, does not preserve any memory of the incoming gamma direction. Nevertheless, it should be noticed that upon photo-electric absorption, once the photo-electron was emitted in a particular direction, the following Cherenkov emission can be directional. However, the directionality of the Cherenkov emission is different for each event, adding to the overall amplitude fluctuation of Cherenkov photons detected. All in all it can be noted that, on average, Cherenkov radiation in heavy scintillators for PET is fairly isotropic, and directional on an event by event basis.

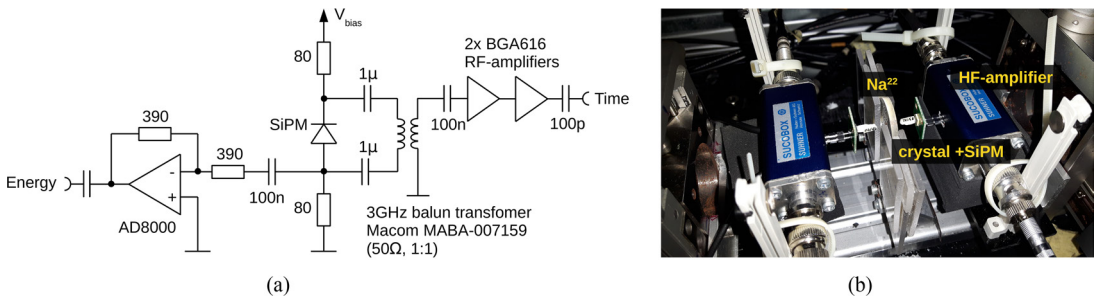

Figure 3. High-frequency SiPM readout. (a) Schematics of the HF-amplifier front-end electronics employing two BGA616 bipolar monolithic microwave integrated circuit (MMIC) amplifiers (Gundacker *et al* 2019). (b) Picture of the HF-amplifiers mounted in blue aluminum boxes for proper electric shielding. Two amplifiers are arranged opposite to each other with a ^{22}Na source in the middle to measure the CTR.

3. Methods

This chapter will give an overview of the experimental setups used to measure the CTR and single photon time resolution (SPTR). We further give an overview of the time correlated single photon counting (TCSPC) and Monte-Carlo simulation tools used. This chapter is merely a review of the most important aspects of the setups in order to understand the following experimental findings, as most of the experimental methods are already familiar in literature. Results are given in sections 4 and 5.

3.1. Electronics: high frequency readout

The front-end to read the SiPM signal employs a small radio-frequency (RF) balun transformer monitoring the voltage drop accross the SiPM anode and cathode, as can be seen in figure 3(a). The differential readout circuit was described in Cates *et al* (2018) and is able to read the fast voltage drop across the SiPM without significant bandwidth limitation, allowing for a very fast SiPM single cell signal rise time (significantly lower than 1 ns). In figure 3(a) the front-end was modified to additionally read, with low amplification, the signal seen at the shunt resistor on the SiPM anode. The amplification of this 'energy' signal is unity and can be used to monitor the energy deposited in the scintillator coupled to the SiPM via charge integration or via the voltage amplitude. A more in depth discussion on the used readout electronics can be found in Gundacker *et al* (2019). Figure 3(b) shows the implementation of the electronics in properly shielded aluminum boxes, allowing to couple different SiPMs. In this picture two amplifiers are arranged opposite to each other with a ^{22}Na radioactive source in the middle to measure the CTR in a TOF-PET like system (section 3.2). The two detectors are placed very close (about 5 mm) to the point source with an activity of 280 kBq, in order to increase the count rate. Proper electric shielding is very important in order to avoid oscillations and pick-up noise, especially when using SiPMs with different packaging.

3.2. Coincidence time resolution measurement setup

The CTR was measured with the standard setup discussed in Gundacker *et al* (2019) and other publications. A ^{22}Na source emits two back-to-back 511 keV gammas which are detected in coincidence by the crystals coupled to the SiPMs. The SiPM signal is amplified by the HF-electronics for the time signal and the analog operational amplifier for the energy signal. The HF-signals are digitized by a LeCroy DDA735Zi oscilloscope with 3.5 GHz bandwidth and a sampling rate of 40 Gs s^{-1} (using four channels this reduces to 20 Gs s^{-1}, i.e. 50 ps binning). The leading edge threshold is set on the oscilloscope to calculate the signal crossing time of both high-frequency channels via linear interpolation, giving the coincidence delay times. The energy was determined by charge integration of the analog SiPM signal with no amplification, performed on the oscilloscope. The acquired data, in form of text files, were analysed offline (with Matlab) to select events within the two photopeaks. The applied photopeak selection on the energy spectra was in the $(\mu - 1.5\sigma, \mu + 2\sigma)$ range. However, the exact photopeak selection window is changing only marginally the obtained CTR. The corresponding delay times were plotted in a histogram and a Gaussian fit was performed using Matlab.

As mentioned before, the delay times were obtained by a leading edge threshold discrimination (done by the oscilloscope) applied on the high frequency channels, which was scanned in a broad range from threshold values just above the electronic noise floor ~2 mV to ~140 mV. The single SPAD signal amplitude is about 40 mV. Every CTR measurement in this threshold scan is statistically independent, which allows to reduce the statistical uncertainties by fitting the CTR as a function of the leading edge threshold value (x) with the equation $CTR_{fit} = \sqrt{p_1 x^{p_2} + p_3/(x^{p_4}) + p_5}$, where p_i denotes the fit parameters. The minimum of this fit, prior to visual inspection, is reported as the CTR in full width at half maximum (FWHM). The oscilloscope time axis was

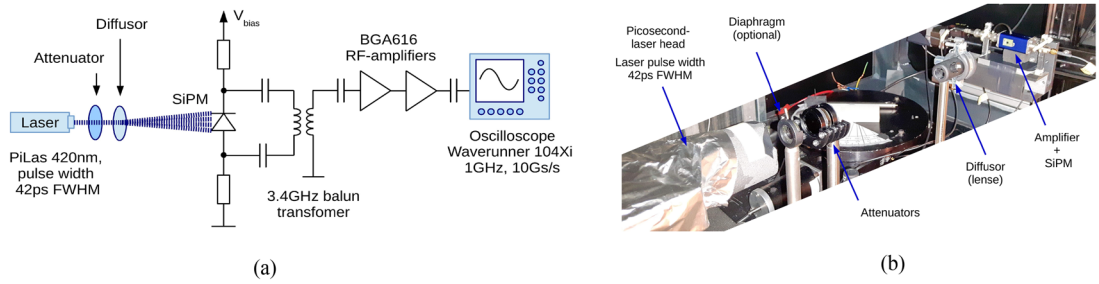

Figure 4. Single photon time resolution measurement setup. (a) Sketch of the single photon time resolution SPTR setup. (b) Picture of the SPTR setup used. The laser head is shielded with aluminum foil in order to minimize high-frequency pick-up in the amplifier electronics.

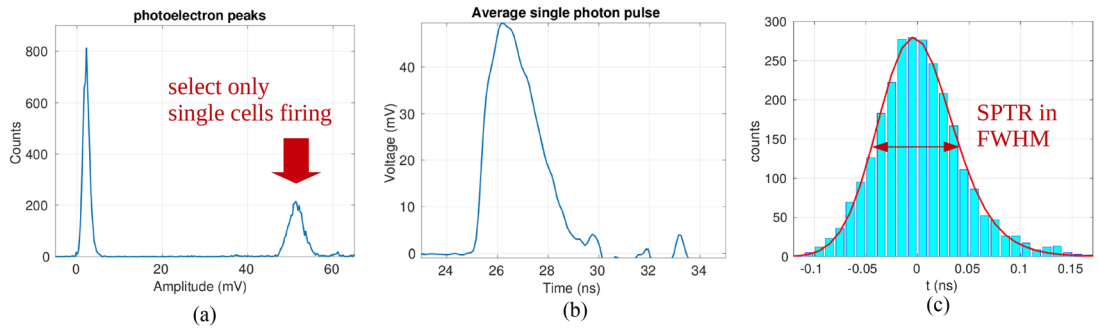

Figure 5. Data analysis of the single photon time resolution measurements. (a) Amplitude histogram of the SiPM signal with single photon event selection. (b) Example of an average single photon (SPAD) signal obtained with FBK NUV-HD showing a maximum $dV/dt = 90$ mV ns^{-1}. (c) SPTR histogram with the value given in FWHM from a fit including possible tails.

calibrated by the manufacturer, but we tested this calibration by moving the ^{22}Na source for a known distance and measuring the corresponding change in the delay times (see Gundacker *et al* (2019) for more information).

3.3. Single photon time resolution measurement setup

We measured the single photon time resolution (SPTR) of the different SiPMs with the high-frequency electronics introduced in section 3.1. The electronics and setup are very similar to the ones reported in Cates *et al* (2018), we only modified the HF-amplifier using a BGA616 monolithic microwave integrated circuit (MMIC) from Infineon instead of a MAR-6 from Mini-circuits, and took care of proper electric shielding of the amplifier and laser-head plus driver in order to minimize pick-up noise. A sketch of the setup can be seen in figure 4(a) and a picture of the setup in figure 4(b). A 420 nm picosecond laser from PiLas was used with a laser pulse width of 42 ps FWHM, verified by a streak camera (Nemallapudi *et al* 2016). We always operated the laser at 50% intensity and a repetition rate of 10 kHz. To adjust the laser intensity we used optical attenuators (absorptive ND filters of Thorlabs) and diffused the laser beam to illuminate the whole active area of the SiPM. The amplified signal is digitized with a LeCroy oscilloscope Waverunner 104Xi with 1GHz bandwidth and 10 Gs s^{-1} sampling rate. In the offline data-analysis we select only single photon events (see figure 5(a)) and perform a baseline subtraction and spline interpolation of the recorded laser trigger and SiPM signal. We apply leading-edge discrimination to the interpolated signal and scan the threshold to find the minimum SPTR value, which most of the times is in the first half of the single cell amplitude. In figure 5(b) we show the average single cell signal for a FBK NUV-HD SiPM, 4 × 4 mm^2 area, 40 μm SPAD size and no-resin entrance window. The HF-electronics is able to deliver a very clean and fast signal, in this particular case the 10% to 90% signal rise time is ∼700 ps, which gives a maximum slew-rate of $dV/dt = 90$ V μs^{-1} or $dV/dt = 90$ mV ns^{-1}. With the amplifier noise floor at 1.07 mV rms (SiPM connected), this implies that the noise contribution to the SPTR, $\text{SPTR}_{noise} = 1.07$ mV/(90 mV ns^{-1}) = 12 ps rms, or 28 ps FWHM. In the data analysis we apply a fit including tails, as described in Nemallapudi *et al* (2016). This fit function was then used to calculate the full width at half maximum of the recorded data (to be seen in figure 5(c)). Hence, SPTR values are always given in FWHM.

In figure 6 we list the individual contributions which the measured $\text{SPTR}_{measured}$ is composed of. The intrinsic $\text{SPTR}_{intrinsic}$ is the important parameter for understanding the measured CTR with scintillators and Cherenkov radiators. To correctly determine the intrinsic SPTR of the photodetector we need to deconvolve from the measured SPTR the laser pulse width, laser trigger jitter, acquistion jitter (e.g. of the oscilloscope) and electronic noise

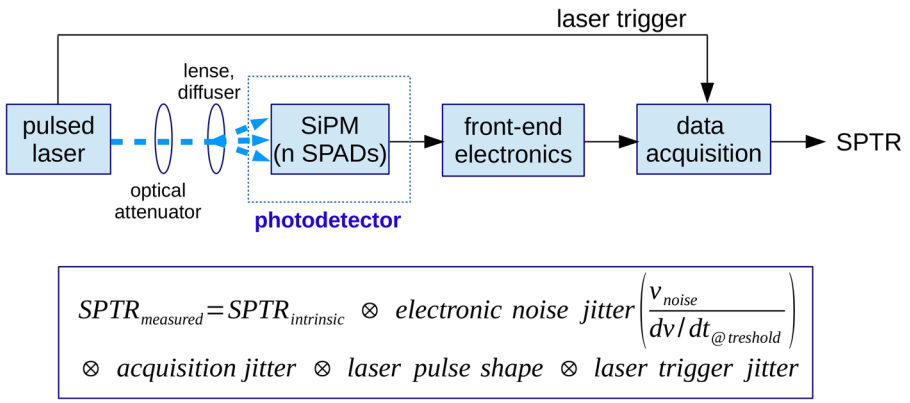

Figure 6. Defining the intrinsic SPTR. The measured SPTR value is a convolution of the laser pulse, electronic noise and acquisition jitter. The laser pulse shape is Gaussian with 42 ps FWHM.

jitter ($SPTR_{noise} = 2.35 \cdot v_{noise}(\mathrm{rms})/(dv/dt_{@threshold})$). The laser trigger jitter was found to be only a few picoseconds and hence negligible, similar to the acquisition jitter of the used LeCroy oscilloscope.

3.4. Time correlated single photon counting (TCSPC) setup

The scintillation emission kinetics of the studied scintillators were measured with a time correlated single photon counting (TCSPC) setup (Bollinger and Thomas 1961), either with x-ray or 511 keV gamma excitation. In the case of 511 keV excitation we used a setup very similar to the one described in Seifert *et al* (2012), Gundacker *et al* (2016b). The only difference is, that we accept all events regardless of the energy deposition in the crystal under test. Further, we used different stop detectors suited to the emission of the scintillation, e.g. ID-Quantique (IDQ) ID100-50 (a single photon avalanche diode) for BGO, or VUV-SiPMs for BaF_2. Scintillation kinetic studies with x-ray excitation have been done using a Hamamatsu N5084 x-ray tube with a maximum energy of 40 keV (Gundacker *et al* 2018). As stop detector we used a hybrid-PMT (HPM-100-07 from Becker&Hickl) read out by a fast 8 ps resolution time-to-digital converter (Cronologic xTDC4). The quantum efficiency of the hybrid-PMT is reported for values down to 220 nm only, with a noticeable drop in efficiency in the vacuum ultraviolet (VUV). This has to be taken into account when studying the emission around 200 nm, for this could lead to an underestimation of the amplitude in this wavelength range (e.g. for BaF_2).

3.5. Monte Carlo simulation framework

In this paper we will focus on Monte-Carlo (MC) simulations with LSO:Ce:Ca and BGO, read out by FBK NUV-HD SiPMs of 4×4 mm^2 active area and 40 μm SPAD pitch (Piemonte *et al* 2016). As input parameters we take the measured scintillation rise times, decay times, ILY, SiPM photon detection efficiencies weighted for the scintillation emission and SiPM single photon time resolution, as discussed in Gundacker *et al* (2019) and in this paper in the following chapters.

The MC simulations have been performed in the same spirit as already described to large extent in several of our previous publications (Gundacker *et al* 2013, 2014, 2015, Acerbi and Gundacker 2019). We also include optical photon transport in the crystal, always fully wrapped in Teflon and coupled to the SiPM with a high-refractive index glue (Gundacker *et al* 2014). The optical photon tracking was done by SLitrani, including imperfections of the scintillator, like non-perfect surface polishing and absorption (Knapitsch 2012). In the case of simulating the analog SiPM timing, we superimpose the SiPM single cell signals at the photon detection times determined by Monte-Carlo (Gundacker *et al* 2015). An example of a single cell (SPAD) signal is shown in figure 5(b), this signal can be described by a multi-exponential with its own rise and decay time (Acerbi and Gundacker 2019). We additionally include a long undershooting tail caused by the high-pass filter placed at the amplifier output in order to suppress baseline fluctuations. The bandwidth limitation of the electronics was taken into account by a butterworth low pass filter of first order with a cut-off frequency of 1.5 GHz (Gundacker *et al* 2019), applied after the single SPAD signal pile-up. In order to mimic the correct single cell signal rise time after this low pass filtering, we set the intrinsic SiPM single SPAD rise time to $\tau_{\mathrm{SPAD}\,rise} = 400$ ps.

For the particular MC simulations in this work we do not include optical crosstalk in the SiPM, which we noticed to be of lower importance if SiPMs with low SPTR values are considered. It has to be mentioned that the Monte-Carlo simulations naturally include effects like the 511 keV gamma depth of interaction (DOI) in the crystal. This is well known to become progressively important in the case of ultrafast timing in the 50 ps range for long crystals, e.g. L(Y)SO:Ce(:Ca) with 20 mm length.

Furthermore, we used the MC simulation tool to study the expected timing performance with a multi-digital SiPM, when every single time stamp of the cascade of detected photons is recorded (Fishburn and Charbon 2010). For the case of LSO:Ce:Ca we combine the obtained simulated time stamps via a maximum likelihood estimator (MLH), described in Gundacker *et al* (2015), which is basically a weighted average of the photon time stamps. For simulations of BGO and the detection of Cherenkov photons we simplified the digital readout to take only the first detected photon into account, producing the best timing in this particular case.

Prompt (Cherenkov) photons emitted in the scintillator are included using the correctly weighted PDE of the SiPM for the scintillation and Cherenkov emission, respectively. For LSO:Ce:Ca we incorporate an average number of 7 and for BGO 17 Cherenkov photons produced for each 511 keV gamma absorption. For BGO this value is measured in the 310–850 nm range (transparency window of BGO), for which we refer to section 5.2 of this paper. For LSO:Ce:Ca the mean value of 7 Cherenkov photons in the 390–750 nm range is estimated with Geant4 simulations. Further, we included an additional 30% amplitude fluctuation of the emitted Cherenkov photons around the stated mean values due to the stochastic electron path (indicated by Geant4 simulations), which is on top of the naturally included Poisson-fluctuation caused by the finite PDE and LTE.

4. SiPM timing performance of different devices

In this chapter we give an overview of the best SiPM timing achievable with state-of-the-art industrial and research devices. We will focus on the single photon time resolution (SPTR) measured with a picosecond-laser and present an estimate of the intrinsic SPTR of the devices. Further we will couple our test crystal, a $2 \times 2 \times 3$ mm^3 LSO:Ce codoped with 0.4% Ca from Agile, to all SiPMs and measure the CTR. In the last part of this section we will show how the intrinsic SPTR influences the best measured CTR in analog SiPMs with high-frequency readout and compare the measurements with comprehensive Monte-Carlo simulations.

4.1. Intrinsic SPTR

The measured SPTR obtained with the different SiPM devices as a function of the overvoltage can be seen in figure 7(a). The values represent the measured SPTR with the contribution of laser pulse width, electronic noise and acquistion jitter, as described by the equation of figure 6. However, in order to know the real intrinsic SPTR of the tested SiPMs we quadratically subtract these additonal known terms. The results are shown in figure 7(b). All SPTR data were taken by illuminating the entire active SiPM area of 4×4 mm^2 or 3×3 mm^2 uniformly. It can be seen that, in terms of intrinsic SPTR, FBK NUV-HD with 4×4 mm^2 active area and 40 μm SPAD size is superior than the other tested SiPMs. This FBK SiPM achieves an intrinsic SPTR of 70 ps FWHM. This is an important achievement for analog SiPMs, even more so under the aspect that the whole active area of 4×4 mm^2 of the SiPM was illuminated uniformly. By illuminating, e.g. only a small area of 1×1 mm^2 of this FBK NUV-HD SiPM we did not notice a significant improvement in SPTR, meaning that at these SPTR values the signal transfer time skew is still of less importance for this device. On the other hand, when we measured two different SiPMs from HPK, i.e. S13360 and S14160 with 3×3 mm^2 active area and 50 μm SPAD size each, we obtained an intrinsic SPTR of 135 ps and 117 ps FWHM, respectively. The higher SPTR values of the HPKs compared to the FBK SiPMs are most likely explained by a different electric field distribution in the SPADs (Nemallapudi *et al* 2016, Acerbi and Gundacker 2019). The better performance of the HPK S14160 as compared to the HPK S13360 can be explained by a reduced signal transfer time skew in that device, probably caused by the central wire connection. A picture of the device is shown in figure 1(a). This assumption is corroborated by measuring the SPTR of the S13360 with 3×3 mm^2 active area and 50 μm SPAD size using a 1×1 mm^2 mask, which indeed yields an intrinsic SPTR similar to the one of the S14160 SiPM.

Looking at figure 7(b) it is interesting to notice that the intrinsic SPTR is to a large extent independent of the overvoltage if the overvoltage is above 3–5V. A possible explanation is that the electric field at these overvoltages already penetrates the whole SPAD, showing spatial saturation, especially at the edges. Here it can be seen that devices with a lower breakdown voltage and, hence, commonly thinner depletion region (e.g. FBK, Ketek, SensL), do reach this saturation point at noticeably lower overvoltages. This behaviour goes hand in hand with a similar observation in figure 1, where the PDE as well saturates at around 3–5 V overvoltage. We want to stress that, at very low overvoltages the intrinsic SPTR potentially can be much worse as compared to high overvoltages, already indicated by figure 7(b). For PET applications where the SiPMs can be operated at high bias voltages this observation is of secondary importance, but might need further revision and attention in high energy physics where the SiPM has to be operated close to its breakdown voltage in order to minimize the dark count rate induced by radiation damage (Garutti and Musienko 2019).

4.2. CTR with LSO:Ce:Ca

In figure 8 an example of the CTR as a function of the leading edge threshold can be seen, for the case of FBK NUV-HD with 40 μm SPAD size. The figure shows results obtained with $2 \times 2 \times 3$ mm^3 LSO:Ce:0.4%Ca as well

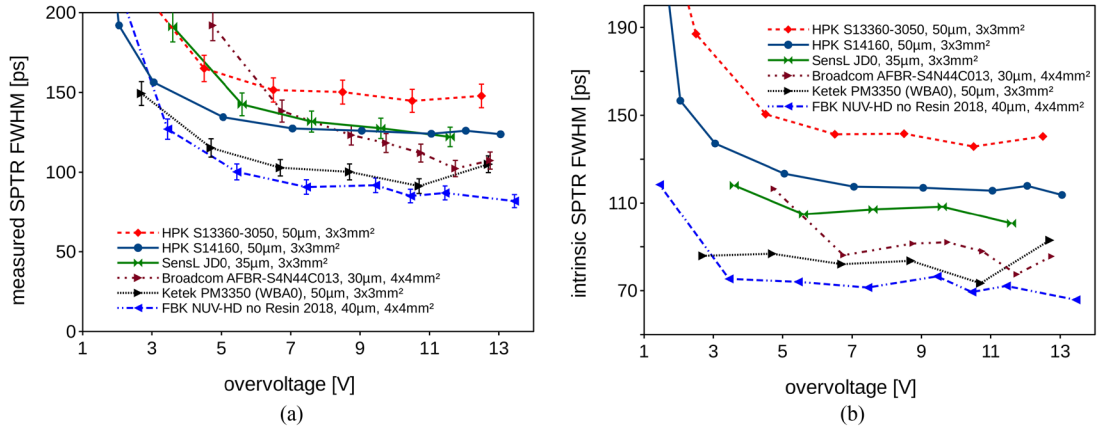

Figure 7. Measured single photon time resolution of HPK, SensL, Broadcom, Ketek and FBK SiPMs. (a) Measured SPTR of the various SiPMs tested, including the picosecond laser pulse width and electronic noise. Measured SPTR values are always derived from uniformly illuminating the entire active SiPM area. (b) Intrinsic SPTR of the various SiPMs: electronic noise contribution and laser pulse width of 42 ps FWHM are subtracted in quadrature.

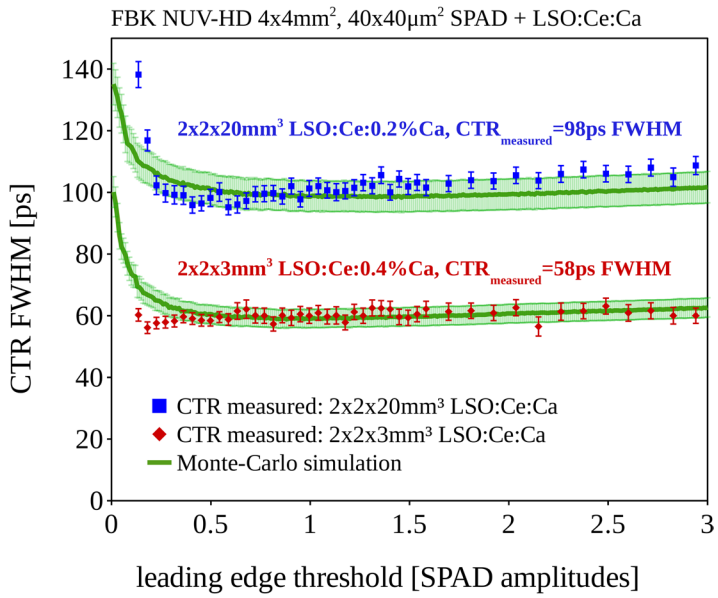

Figure 8. Measured CTR compared to Monte Carlo simulations for FBK NUV-HD coupled to LSO:Ce codoped with Ca. The simulations also include 7 prompt photons produced at the onset of the scintillation process in the range of 390–750 nm.

as the performance with $2 \times 2 \times 20$ mm^3 LSO:Ce:0.2%Ca crystals, achieving their highest CTR at 58 ps and 98 ps FWHM, respectively (Gundacker *et al* 2019). The green solid lines indicate the CTRs expected from the corresponding Monte-Carlo simulations, predicting the measured CTR with high accuracy (the MC simulation error-bars of 5% are shown as well). These MC simulations use the scintillation kinetics as input parameters and the light yield as published in Gundacker *et al* (2018, 2019). For the intrinsic SPTR we use the previously derived value of 70 ps FWHM shown in figure 7. The detection efficiency of the SiPM was determined by weighting the SiPM PDE with the LSO:Ce:Ca emission spectra (see figure 2), which gives a value of 59%. Additionally we take the coupling of the crystal to the bare SiPM with the high refractive index glue (Meltmount $n = 1.582$) into account, leading to an additional gain of ∼1.1 in the number of photons detected (or in the LTE). Furthermore we include an average number of 7 Cherenkov photons produced in the range of 390–750 nm with a weighted PDE of 42%, also multiplied by 1.1 due to the direct high refractive index coupling.

4.3. Overview of best SPTR and CTR achieved with various producers

Table 4 gives a summary of the best CTR values achieved with the various SiPMs under test. The bias voltages, found to give the best PDEs and CTRs (stated in table 1), were then used to determine the SPTR and weighted PDE values given in table 4. It should be noted that the SiPM bias giving the best SPTR and PDE naturally coincides with the bias voltage leading to the highest CTR.

Table 4. SiPM timing performance overview of different state-of-the-art devices. Shown CTR values are the minimum values obtained, with $2 \times 2 \times 3$ mm^3 LSO:Ce:0.4%Ca crystals, at the proper SiPM bias voltage for which the SPTR and PDE values are given. Errors for the PDE weighted with the LSO:Ce:Ca emission (weighted PDE) are in the range of 5%.

SiPM producer	$SPTR_{meas.}$ FWHM (ps)	$SPTR_{noise}$ FWHM (ps)	$SPTR_{intr.}$ FWHM (ps)	Weighted PDE (%)	CTR (ps) FWHM
HPK S13360	144 ± 7	27 ± 3	135 ± 8	59	75 ± 3
HPK S14160	126 ± 5	21 ± 3	117 ± 6	56.5	74 ± 3
Ketek PM3325	184 ± 8	80 ± 4	161 ± 9	53	86 ± 3
Ketek PM3350	92 ± 5	35 ± 3	74 ± 6	51	70 ± 3
SensL FJ30035	132 ± 6	64 ± 4	108 ± 7	50	76 ± 3
Broadcom	112 ± 5	55 ± 3	88 ± 6	55	69 ± 3
FBK NUV-HD	92 ± 5	45 ± 3	68 ± 6	59	63 ± 3
FBK NUV-HD **no resin**	85 ± 5	28 ± 3	69 ± 6	59	58 ± 3

4.4. Importance of the intrinsic SPTR to correctly model the CTR

As already stated before, the 'real' intrinsic SPTR of the SiPM is a very important parameter in order to correctly model and understand the CTR in a TOF-PET system. In table 4 we can see that the different SiPM devices tested by us have a large variation in intrinsic SPTR values ranging from 68 ps to 161 ps FWHM. Hence, the different measured SPTRs for the different SiPM devices tested by us allow us to draw conclusions of the SPTR influence on the CTR. Also the weighted PDEs are slightly different for the different SiPMs, which can be accounted for by pure photostatistics, since the CTR is inversely proportional to the square root of the PDE (CTR $\propto 1/\sqrt{\text{PDE}}$). Summarizing the values in table 4 we can make a correlation plot of the CTR (normalized to a PDE of 59%) versus the intrinsic SPTR, as shown in figure 9. It can be seen that the measured CTR is almost linearly dependent on the intrinsic SPTR. In figure 9 the green solid line (with 5% error) represents Monte-Carlo simulations of the CTR obtained with high-frequency readout of an analog SiPM, as described before in section 3.5. In addition to the scintillation photons, we take also 7 Cherenkov photons produced into account, emitted within 390–750 nm detected with a weighted PDE of 42%, and furthermore 30% amplitude fluctuations due to the stochastic electron path on top of the Poisson-fluctuation by random deletion (PDE · LTE $\leqslant$ 1). We wish to emphasize once more, that figure 9 highlights the intrinsic SPTR as being an important input parameter to correctly model and understand the CTR in any theoretical calculation.

5. Timing performance of various fast emitting scintillators

This section will give an overview of the timing achievable with different scintillating materials, focussing on BGO, plastic scintillators and BaF_2. All three materials have very different mechanisms of fast photon emission, i.e. Cherenkov emission in BGO, deep-UV cross-luminescence in BaF_2 (Laval *et al* 1983) or fast molecular de-excitations in plastic scintillators. Today, the development of fast SiPMs makes it possible to gauge the performance of these and other materials like L(Y)SO:Ce(:Ca) or CsI:undoped, which will be summarized at the end of the section in a table and an overview plot, with a view on theoretical considerations of the time resolution.

5.1. BGO and prompt photon emission

In figure 10 we show the measured scintillation characteristics of BGO recorded with a time correlated single photon counting (TCSPC) setup described in Gundacker *et al* (2016b). As stop detector we used an ID100-50 sensor from ID-Quantique (IDQ), a single Geiger-mode avalanche photodiode with a size of $50 \times 50\ \mu$m^2 and a single photon time resolution (SPTR) of 94 ps FHWM. The impulse response function of the whole setup, including the data acquisition and the start detector is 148 ps FWHM. It can be seen that in addition to the known BGO emission with decay times of 45.8 ns and 365 ns (see left hand side of figure 10) a prompt peak is visible at the very beginning of the photon-emission (right hand-side of the figure), which is caused by Cherenkov emission. Here, we measured the BGO intrinsic scintillation rise time to be of the order of 8 ps, which is in fact limited by the intrinsic resolution of our setup and within the measurement errors.

Due to the fast slew rate of the electronic signal delivered by the high-frequency readout it is possible to exploit this faint prompt photon emission in BGO (Cates and Levin 2019). An example of the measured CTR with BGO from the producer SICCAS can be seen in figure 11. Experiments were performed with FBK NUV-HD 4×4 mm^2, $40 \times 40\ \mu$m^2 SPAD size and $2 \times 2 \times 3$ mm^3 and $2 \times 2 \times 20$ mm^3 BGO, wrapped in Teflon and coupled with Meltmount ($n = 1.582$). A best CTR of 158 ± 3 ps and 277 ± 3 ps FWHM was achieved for the 3 mm and 20 mm long crystals, respectively.

These results are better than those reported by Kwon *et al* (2016) and Brunner and Schaart (2017), the latter obtained with the Philips digital SiPM. This can mainly be explained by the very high slew rate and bandwidth

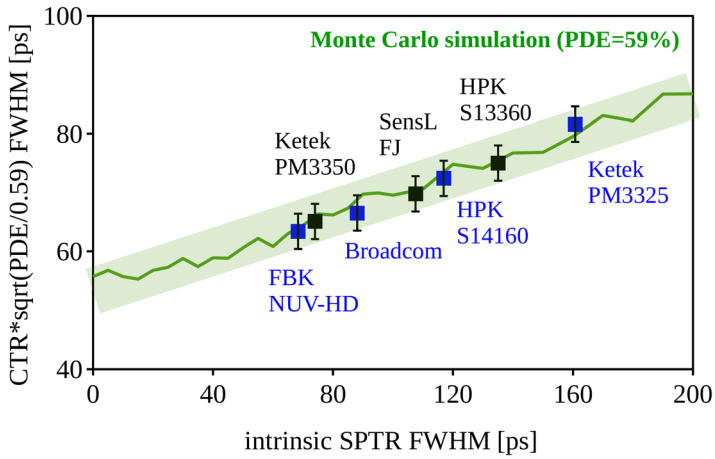

Figure 9. PDE-adjusted CTR as a function of the SPTR. CTR was measured with $2 \times 2 \times 3$ mm^3 LSO:Ce:0.4%Ca crystals wrapped in Teflon coupled with Meltmount and normalized, as if all the SiPMs had a PDE of 59%. Monte Carlo simulations of the CTR with high-frequency readout of an analog SiPM have been performed with the scintillation emission weighted PDE of 59%.

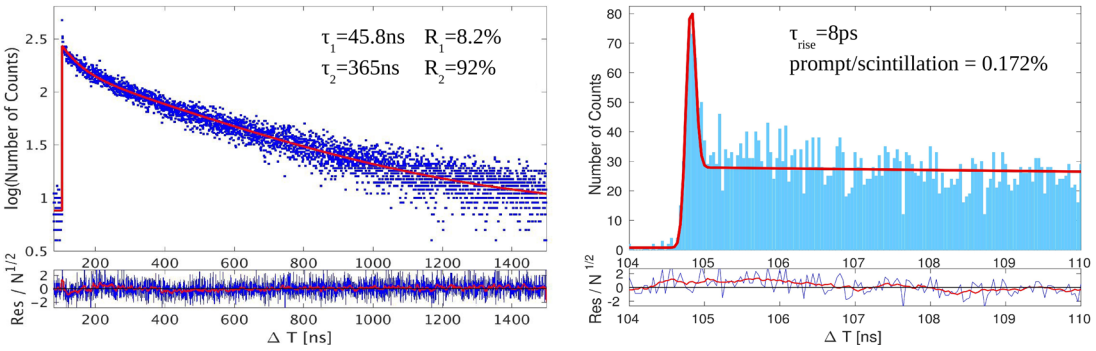

Figure 10. Scintillation decay and rise time of BGO measured with a time correlated single photon counting (TCSPC) setup using 511 keV annihilation gammas (Gundacker *et al* 2016b). The figure on the right hand side shows a pronounced Cherenkov peak at the onset of the scintillation emission with a relative abundance of 0.172% compared to the total amount of photons detected by the stop detector of the TCSPC setup.

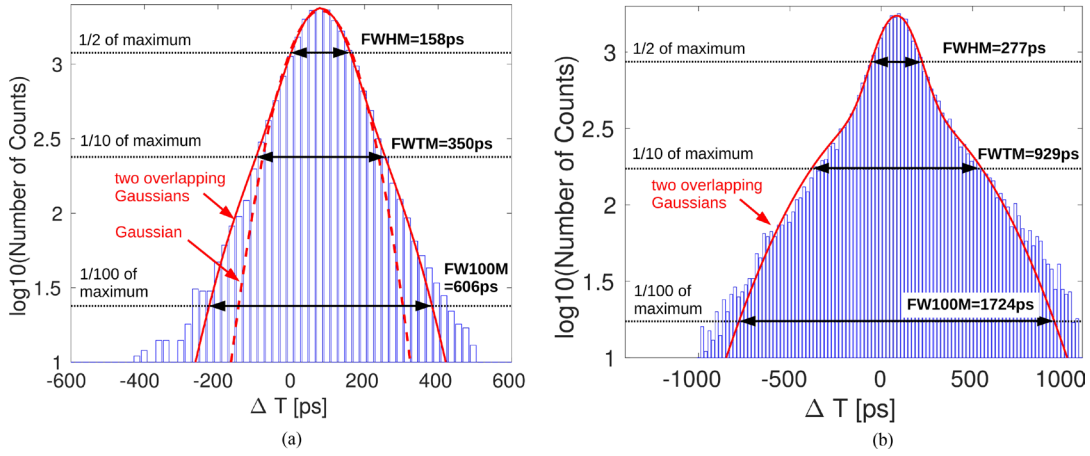

Figure 11. CTR achieved with BGO coupled to FBK NUV-HD SiPMs. (a) Delay time histogram measured at 10 mV leading edge threshold resulting in a CTR of 158 ps FWHM with $2 \times 2 \times 3$ mm^3 BGO coupled to NUV-HD 4×4 mm^2 SiPMs, 40 μm SPAD size. Shown is a Gaussian fit to the data (dotted red line) and a fit of two overlapping Gaussians (solid red line). (b) CTR measured for a similar BGO crystal with $2 \times 2 \times 20$ mm^3 size resulting in a CTR of 277 ps FWHM.

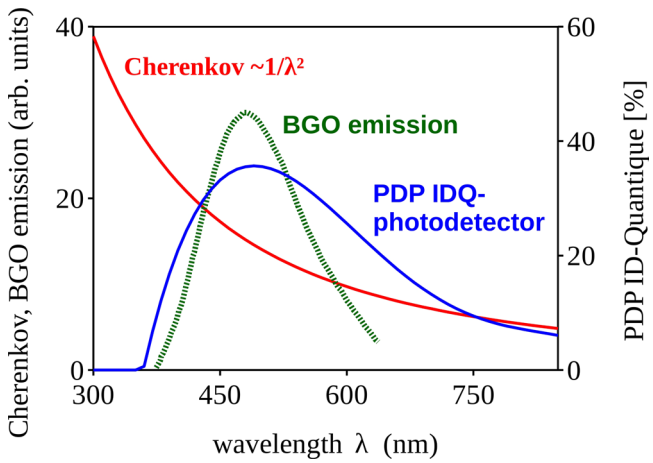

Figure 12. Cherenkov and BGO emission together with the photon detection probability (PDP) of the used ID100-50 SPAD photodetector as a function of the wavelength λ.

Table 5. Summary of the measured number of prompt photons produced in BGO and LuAG:Pr. 'Ch.' stands for Cherenkov, 'scint.' for scintillation and PDP for the photon detection probability of the used stop-detector in the TCSPC setup. In the error estimation we assume 10% error for the ILY and 10% error for the measured Cherenkov/scintillation ratio, which gives an overall uncertainty of 20%.

crystal	ILY scint. (ph MeV^{-1})	Ch./scint. ratio (%)	PDP (%) scint.	Ch. range (nm)	PDP (%) Ch.	Ch. photons produced
BGO	**10 700**	**0.172**	**31.6**	**310–850 nm**	**17.6**	**16.9 ± 3**
LuAG:Pr	22 000	0.351	5.3	300–850 nm	16.7	12.4 ± 3

of the high-frequency readout system (Gundacker *et al* 2019), as was as well shown by Cates and Levin (2019). In figure 11 we also observe that such readout in large part suppresses long tails in the CTR histogram as compared to former studies (Brunner and Schaart 2017), implying that the time stamps are mostly generated by prompt photons and not by the intrinsic BGO scintillation.

We furthermore tested BGO from another producer, Epic-crystals, and found a CTR of 167 ± 3 ps FWHM for 3 × 3 × 3 mm^3 and 235 ± 5 ps FWHM for 3 × 3 × 15 mm^3 size crystals coupled to NUV-HD SiPMs with Meltmount ($n = 1.582$), wrapped in Teflon and applying time walk correction. These results are of great interest and very promising for the application of BGO in time of flight PET, as the time resolution achievable with these crystals approaches the performance of state-of-the-art scanners with current values of 210 ps FWHM for the Siemens Biograph vision (Conti and Bendriem 2019).

5.2. Measuring the number of Cherenkov photons produced in BGO

In order to fully understand the potential of BGO for TOF-PET it is important to estimate the number of prompt (Cherenkov) photons produced in the scintillator. One way is via Geant4 simulations including the measured refractive index of BGO versus the wavelength (Williams *et al* 1996). Such simulations lead to a mean number of 18.8 Cherenkov photons emitted in the 310–750 nm range by an electron with initially 420 keV kinetic energy (511 keV minus the Bismuth K-shell binding energy). Additionally, these simulations can provide the histogram of the number of Cherenkov photons emitted, which is almost Gaussian with a standard deviation of 5.6 photons. This 30% amplitude fluctuation is indeed important for Monte-Carlo simulations in order to include correctly the excess noise factor on the time resolution.

In addition to the Geant4 simulations one can also measure the number of produced Cherenkov photons in a scintillator. With a precise TCSPC setup it is possible to measure the relative intensity of prompt photons recorded to the whole scintillation emission, as shown in figure 10. The measured prompt/scintillation ratio is 0.172% for the case of BGO (figure 10) and 0.351% for LuAG:Pr (Gundacker *et al* 2016b). In order to extract the exact number of prompt photons produced we have to know the photon detection probability (PDP) of the stop detector, in our case the ID100-50 sensor from ID-Quantique, the wavelength dependence of the Cherenkov radiation and BGO (LuAG:Pr) scintillation emission, as well as the respective intrinsic light yields. In figure 12 we show the scintillation emission of BGO centered at around 480 nm, the Cherenkov radiation with its characteristic $1/\lambda^2$ shape as a function of the wavelength λ and the photon detection probability of the used stop detector versus the wavelength. The PDP of the ID100-50 SPAD was measured in our laboratory with the same setup used to measure the PDE of the different SiPM samples and described in Acerbi and Gundacker (2019). Hence, we obtain the weighted PDP of our stop detector for the whole scintillation and Cherenkov emission over a given

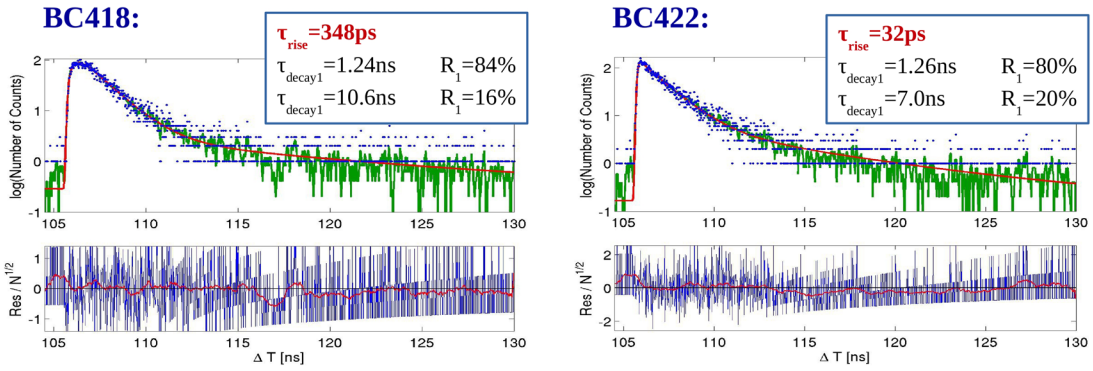

Figure 13. Scintillation kinetics of plastic scintillator BC418 and BC422. Both scintillators exhibit very similar decay times and light yield, with a distinct difference in the scintillation rise time. Measured with 511 keV excitation and TCSPC, as described in Gundacker *et al* (2016b).

wavelength range, as stated in table 5. The ILY of the scintillators was measured with a PMT, correcting for the quantum efficiency and LTE, as listed in table 3. As the ILY in table 5 is given in photons per MeV (ph MeV^{-1}) we have to multiply this value with 0.511 (gamma energy of 511 keV).

For BGO we obtain an average value of 17 ± 3 Cherenkov photons ($17 = 10\,700 \cdot 0.511 \cdot 0.172/100 \cdot 31.6/17.6$) emitted per each gamma interaction within 310–850 nm (see table 5). We additionally estimated the average number of Cherenkov photons emitted by LuAG:Pr being 12 ± 3 per 511 keV gamma interaction in the wavelength range of 300–850 nm. The Geant4 obtained values of 18.8 for BGO in 310–750 nm and 13.9 for LuAG:Pr in 300–750 nm compare very well with the measured values shown in table 5.

Since in our TCSPC setup we do not select the energy deposited in the BGO crystal we would expect the measured average number of Cherenkov photons to be a bit smaller than the one calculated by our Geant4 simulations, where we only consider photo-electric events which are always producing a recoil electron with 420 keV for BGO (or 448 keV for LuAG:Pr). On the other hand hot-intraband luminescence could increase the measured number of prompt photons (Omelkov *et al* 2018), which are not included in Geant4. Since we measure almost the same number of prompt photons in BGO or LuAG:Pr as estimated by Geant4, though with a rather large error-bar, we cannot, at this time, conclude on the hot-intraband yield with 511 keV excitation. This will be subject to future studies.

5.3. Plastic scintillators: BC418 and BC422

We tested two different plastic scintillators (BC418 and BC422) from Saint-Gobain. The scintillation emission kinetics are shown in figure 13. Both materials exhibit very similar decay times and ILY (table 3). However, as seen in figure 13, the scintillation rise times are very different with $\tau_r = 348$ ps for BC418 and $\tau_r = 32$ ps for BC422 under 511 keV excitation.

Indeed, this difference in scintillation rise time is the main reason for the very different CTRs achievable with both compounds, being 75 ± 4 ps FWHM for BC418 and 35 ± 2 ps FWHM for BC422 (shown in figure 14). Both scintillators were coupled to FBK NUV-HD SiPMs with 4 × 4 mm^2 active area and 40 μm SPAD size. Furthermore, it can be seen that the fast scintillation emission of BC422 with an effective decay time of 1.5 ns, rise time of 32 ps and light yield of 10 100 ph MeV^{-1} delivers an outstanding CTR of 35 ± 2 ps FWHM with events selected at the sharp Compton edge, only depositing 340 keV in the material (right hand side of figure 14). Such an excellent CTR is due to the use of the high-frequency readout electronics and the state-of-the-art performance of the used FBK NUV-HD SiPM with a weighted PDE of 52% for BC422 and an SPTR of 70 ps FWHM. This is another showcase for the importance of fast scintillation emission for fastest timing in PET. In order not to sacrifice sensitivity in PET, new research tends to combinine fast scintillation emission with high density materials (e.g. CdSe based nanoplatelets) together with 'standard' materials like BGO or LYSO (providing the neccessary 511 keV stopping power) in a metamaterial or hybrid scintillator (Turtos *et al* 2019a, 2019b).

5.4. Cross-luminescence: barium fluoride

Cross-luminescence emission in BaF_2 is known to be very fast, highlighting a ∼600 ps decay time component with a light yield of ∼1500 photons per MeV (Laval *et al* 1983, Lecoq *et al* 2006). Hence, BaF_2 is an interesting candidate for fastest timing in certain PET concepts and for high-energy physics, because its density is decently high, and the crystal can be produced at reasonable cost. However, the fast cross-luminescence emission is a true challenge for photodetectors, as the produced light is emitted in the deep UV, i.e. at 195 nm and 220 nm.

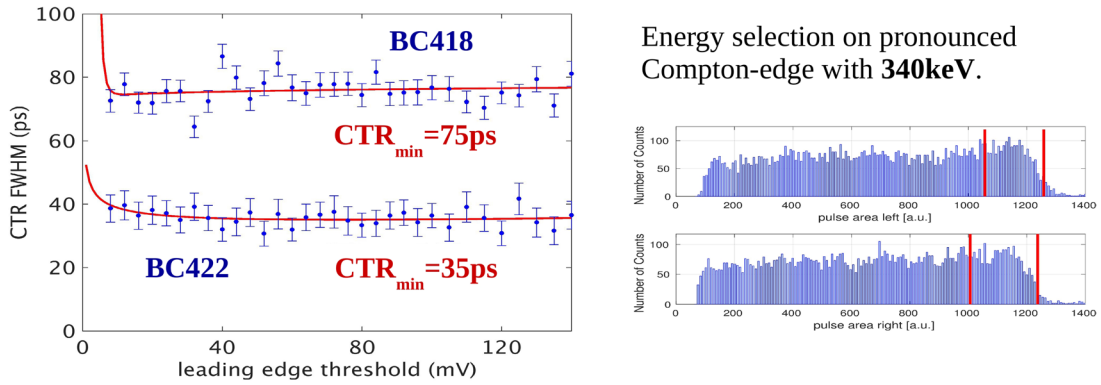

Figure 14. Measured CTR in FWHM of BC418 and BC422 versus the leading edge threshold of the high-frequency and FBK NUV-HD SiPM readout. The faster rise time of BC422 leads to a noticeably better CTR of 35 ps FWHM (left hand side). The CTR was obtained by selecting events at the sharp Compton-edge with only 340 keV energy deposition in the scintillator (right hand side).

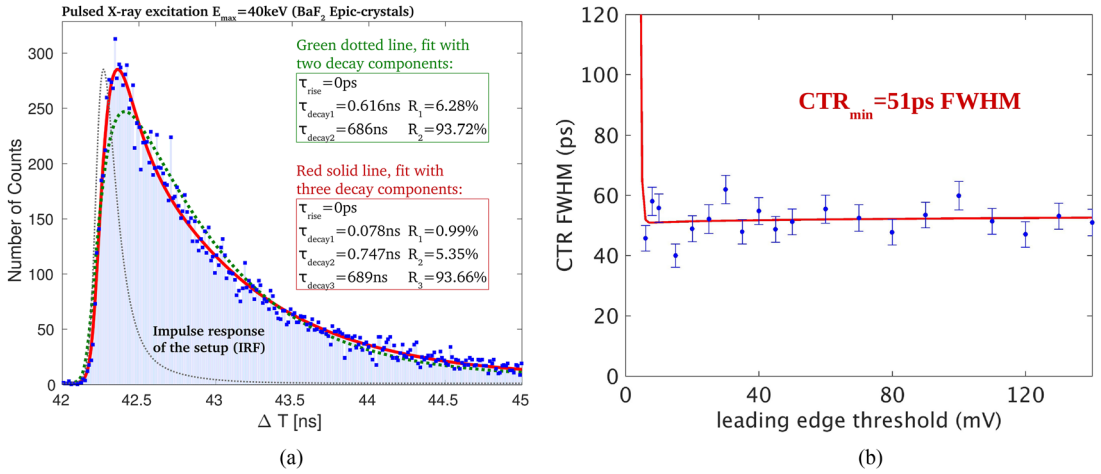

Figure 15. Timing performance of BaF_2. (a) BaF_2 scintillation kinetics in the 220–850 nm range, measured with pulsed x-ray excitation (40 keV maximum energy) (Gundacker *et al* 2018) and a hybrid-PMT (HPM-100-07 Becker&Hickl) as stop detector. (b) Measured CTR of BaF_2 versus the leading edge threshold with the crystal coupled to FBK VUV-HD SiPMs using Glycerin as coupling agent.

To investigate the timing potential of BaF_2 we measured the scintillation kinetics of samples from Epic-crystals under pulsed x-ray excitation (Gundacker *et al* 2018) (maximum energy of 40 keV) and confirmed that a double-exponential decay fit gives a fast decay time of 616 ps with 6.28% relative light yield and 686 ns with 93.72% abundance together with an almost non-detectable rise time, compatible with 0 ps (see figure 15(a)). However, looking closer at the acquired data we notice that we need an additional faster emission in these samples with a decay time of 78 ps and 0.99% abundance to obtain a satisfactory fit. In this case the remaining decay components are 747 ps with 5.35% and 689 ns with 93.66% yield. In our setup we used as stop detector a hybrid-PMT (HPM-100-07 from Becker&Hickl), which has its quantum efficiency reported down to values of 220 nm with about 10%. Hence, the fast components measured are still under investigation and most likely underestimated in their yield.

As already mentioned, the fast emission bands of BaF_2 are located in the deep-UV at 195 nm and 220 nm, which sets severe constraints on the photodetector selection. Recent developments for dark matter search yielded SiPMs with photon detection efficiencies of ∼22% at wavelengths of 200 nm. We tested these new state-of-the-art VUV-HD devices from FBK (Gola *et al* 2019) and measured a CTR of 51 ± 5 ps with 2 × 2 × 3 mm^3 BaF_2 crystals excited by 511 keV gammas, as can be seen in figure 15(b). For these measurements the crystal was coupled to the SiPM with UV-transparent Glycerin. Furthermore, the nowadays moderate PDE values are still leaving room for quite some improvements.

5.5. Overview of measured scintillation kinetics

Table 6 gives an overview of the measured scintillation kinetics for all materials tested, measured with a time correlated single photon counting (TCSPC) setup (Gundacker *et al* 2016b, 2018). The data of LYSO:Ce and LSO:Ce:Ca was taken from our previous publication (Gundacker *et al* 2018) and is shown for comparison with

Table 6. Overview of the scintillators and their characteristics studied in this work. The ILY is again shown for comparison.

Composition	τ_r (ps)	τ_{d1} (ns)	R_1 (%)	τ_{d2} (ns)	R_2 (%)	τ_{d3} (ns)	R_3 (%)	τ_{deff} (ns)[f]	ILY (ph keV^{-1})
LSO:Ce:0.2%Ca[a]	9 ± 9	10.8	5	35.0	95	—	—	31.5	39.2
LSO:Ce:0.4%Ca[a]	10 ± 10	7.5	5	32.4	95	—	—	27.8	32.0
LYSO:Ce[a]	68 ± 20[b]	21.5	13	43.8	87	—	—	38.6	41.1
BGO[c]	8 ± 8	45.8	8	365	92	—	—	234.3	10.7
BaF_2[d]	0 ± 3	0.078	0.99	0.747	5.35	689	93.66	5.0	8.5
BaF_2[e]	0 ± 3	0.627	16.88	698	83.12	—	—	3.7	8.5
CsI:undoped[d]	9 ± 9	0.967	11.5	5.78	30.2	36.3	58.3	5.4	7.2
LuAG:Pr[a]	254 ± 50	22	50	924	50	—	—	43.0	22.0
GAGG:Ce:Mg[a]	72 ± 20	60	66	188	34	—	—	78.1	69.4
GFAG[c]	56 ± 20	43	66	172	34	—	—	57.2	55.7
BC418[c]	348 ± 50	1.24	84	10.6	16	—	—	1.44	12.3
BC422[c]	32 ± 10	1.26	80	7.0	20	—	—	1.51	10.1

[a] Scintillation kinetics from Gundacker *et al* (2018).
[b] More precise: (8 ± 8) ps with $(83 \pm 6)\%$ and (304 ± 120) ps with $(17 \pm 6)\%$ (Gundacker *et al* 2018).
[c] TCSPC with 511 keV excitation and ID-Quantique (IDQ) ID100-50 readout.
[d] TCSPC with x-ray excitation (40 keV) and hybrid-PMT (HPM-100-07 Becker&Hickl) readout.
[e] TCSPC with 511 keV excitation and FBK VUV-SiPM readout, two component decay fit.
[f] The effective decay time is calculated as: $\tau_{deff} = (R_1/\tau_{d1} + R_2/\tau_{d2} + R_3/\tau_{d3})^{-1}$.

Table 7. Overview of the best scintillator timing performance in a TOF-PET system achieved by us.

Material	Center emissions (nm)	Crystal size (mm^3)	SiPM used	Weighted PDE (%)[a]	CTR (ps)
LSO:Ce:0.2%Ca	420	$2 \times 2 \times 3$	NUV-HD 40 μm	59 ± 3	60 ± 3
LSO:Ce:0.2%Ca	420	$2 \times 2 \times 20$	NUV-HD 40 μm	59 ± 3	98 ± 3
LSO:Ce:0.4%Ca	420	$2 \times 2 \times 3$	NUV-HD 40 μm	59 ± 3	58 ± 3
LYSO:Ce	420	$2 \times 2 \times 3$	NUV-HD 40 μm	59 ± 3	69 ± 3
BGO	480	$2 \times 2 \times 3$	NUV-HD 40 μm	47 ± 3	158 ± 3
BGO	480	$2 \times 2 \times 20$	NUV-HD 40 μm	47 ± 3	277 ± 3
BaF_2	195/220 (fast)	$2 \times 2 \times 3$	VUV-HD 40 μm	$\sim 22 \pm 5$[b]	51 ± 3
CsI:undoped	315	$2 \times 2 \times 3$	NUV-HD 40 μm	17 ± 3	90 ± 3
LuAG:Pr	320/370	$2 \times 2 \times 8$	NUV-HD 40 μm	38 ± 3	175 ± 3
GAGG:Ce:Mg	540	$2 \times 2 \times 3$	S13360-3050PE	54 ± 3	88 ± 3
GAGG:Ce:Mg	540	$2 \times 2 \times 3$	NUV-HD 40 μm	33 ± 3	110 ± 3
GFAG	540	$2 \times 2 \times 3$	S13360-3050PE	54 ± 3	85 ± 3
BC418	391	$2 \times 2 \times 5$	NUV-HD 40 μm	57 ± 3	75 ± 3
BC422	370	$3 \times 3 \times 3$	NUV-HD 40 μm	52 ± 3	35 ± 3

[a] The weighted PDE is the SiPM PDE weighted with the scintillation emission of the corresponding material taking into account the cut-off wavelength of the used Meltmount coupling-agent at ~315 nm.
[b] PDE values for the VUV-HD SiPM are taken from Gola *et al* (2019).

the newly measured values. The scintillation kinetics of BaF_2 were measured with x-ray and 511 keV excitation using a hybrid PMT (HPM-100-07 Becker&Hickl) or FBK VUV-SiPM as stop detector, respectively. As already discussed in the preceding chapter, we observe a very fast decay time ~100 ps in addition to the known 600 ps cross-luminescence decay (Laval *et al* 1983). However, the x-ray TCSPC measurements are likely underestimating the relative intensities of the fast components, because of the poor detection efficiency of the used hybrid-PMT in the deep-UV around 200 nm. Preliminary TCSPC measurements with 511 keV excitation and VUV-SiPM readout confirm this assumption. Corresponding values obtained for a two-decay-component fit are shown in table 6. In timing applications a useful figure of merit is the effective decay time $\tau_{deff} = (R_1/\tau_{d1} + R_2/\tau_{d2} + R_3/\tau_{d3})^{-1}$. Here R_i are the relative light yields (normalized to area) of the decay time components τ_{di} with $\sum_i R_i = 1$.

5.6. Overview of best scintillator timing achieved

Table 7 gives a summary of the best CTR obtained for all tested scintillators. Most of the time we took FBK NUV-HD SiPMs to read the scintillation light, except for GAGG:Ce:Mg and GFAG, where SiPMs from HPK are more

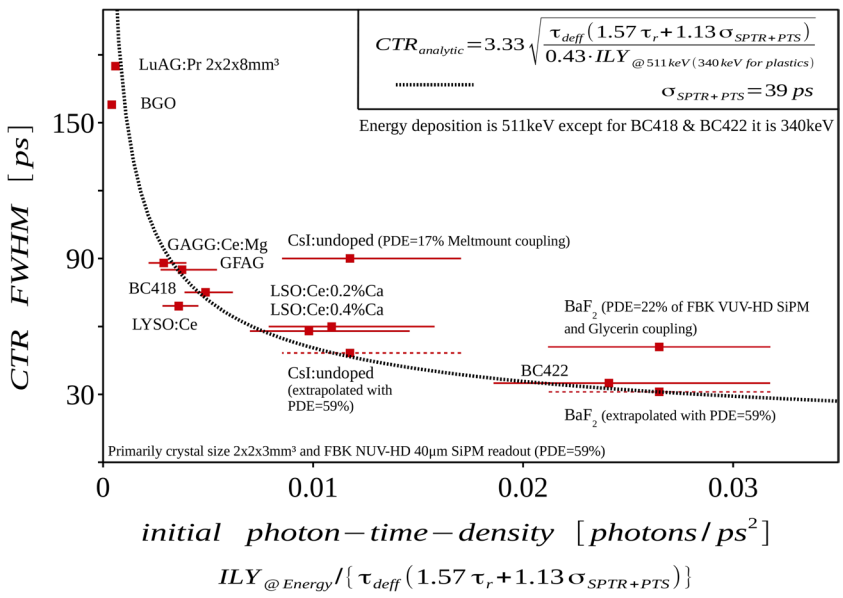

Figure 16. Best measured CTR (y-axis) for each scintillator tested as a function of the intrinsic timing capability coupled to state-of-the-art SiPMs, given by the scintillation emission initial photon-time-density, on the x-axis. The black dashed line shows an analytic CTR model published by Vinogradov (2018). The ILY multiplication factor 0.43 accounts for the LTE in the crystal and the PDE of the SiPM. Error-bars are mostly given by the uncertainties in the rise time and by a typical uncertainty of 10% in the τ_{deff}/LY parameter.

suited because of their higher PDE at 540 nm (Acerbi and Gundacker 2019). To sense the vacuum ultraviolet emission of BaF_2 we used VUV-HD SiPMs from FBK and Glycerin coupling, as discussed in the preceding section.

To arrange and interpret the vast amount of measurements we summarize the data of table 7 in figure 16 showing the measured CTR as a function of the crystals' initial photon-time density (IPTD) and, hence, the intrinsic timing capabilities of the scintillators. In the work of Vinogradov (2018) an analytic expression of the CTR was calculated being basically the inverse of the square root of this initial photon-time density given by equation (1). Here, τ_{deff} is the effective decay time, the scintillation rise time is given by τ_r and the term $\sigma_{\mathrm{SPTR+PTS}}$ denotes the convolution of the single photon time resolution (SPTR) of the SiPM with the photon transfer time spread (PTS) of the crystal. $\sigma_{\mathrm{SPTR+PTS}}$ is reasonably well described by a Gaussian with 39 ps sigma (or 92 ps FWHM) for a $2 \times 2 \times 3$ mm^3 crystal coupled to a FBK NUV-HD SiPM with 70 ps FWHM SPTR.

$$\mathrm{IPTD} = \frac{\mathrm{ILY}_{@\,Energy}}{\tau_{deff} \cdot (1.57 \cdot \tau_r + 1.13 \cdot \sigma_{\mathrm{SPTR+PTS}})}. \tag{1}$$

With equation (1) it is easy to write the analytic CTR expression as stated in equation (2) and by Vinogradov (2018).

$$\mathrm{CTR}_{analytic} = 3.33 \cdot \sqrt{\frac{\tau_{deff} \cdot (1.57 \cdot \tau_r + 1.13 \cdot \sigma_{\mathrm{SPTR+PTS}})}{\mathrm{PDE} \cdot \mathrm{LTE} \cdot \mathrm{ILY}_{@\,Energy}}}$$
$$\mathrm{CTR}_{analytic} = \frac{3.33}{\sqrt{\mathrm{PDE} \cdot \mathrm{LTE} \cdot \mathrm{IPTD}}}. \tag{2}$$

In this expression we take into account the energy deposited in the crystal $\mathrm{ILY}_{@\,Energy}$ (normally 511 keV or 340 keV in the case of BC418 and BC422), since the values in table 3 are given in photons per keV. We furthermore have to take into account the LTE of the crystal which is 73% in the case of a $2 \times 2 \times 3$ mm^3 LSO:Ce:Ca scintillator coupled with Meltmount to the SiPM (including the gain from the direct coupling to the FBK SiPM without resin), and the weighted PDE of the SiPM, which we calculated to be 59% for the LSO:Ce:Ca emission. This leads to a product of LTE $\cdot$PDE $= 0.43$ in the denominator of equation (2). We are aware that this value is only correct for the tested LSO and LYSO crystals, nevertheless, it seems to be a fair approximation for the plastic scintillators and garnets as well, because of their comparable LTE, as shown in table 3. In the case of BaF_2 and CsI:undoped where the weighted SiPM-PDE values are very different from those with L(Y)SO:Ce(:Ca) with 59% (see table 7), we show the expected CTR in figure 16 as if the PDE of the SiPM was 59%. This estimation was calculated considering pure photostatistics, using the square root of the PDE ratios.

It is interesting to notice that the analytic CTR model of Vinogradov (2018) gives a good estimate of the measured time resolution with the high-frequency readout, as seen in figure 16. The small deviation of LYSO:Ce is explained by the measured two-fold rise time, with a significant part (83%) being zero, which is not accounted for

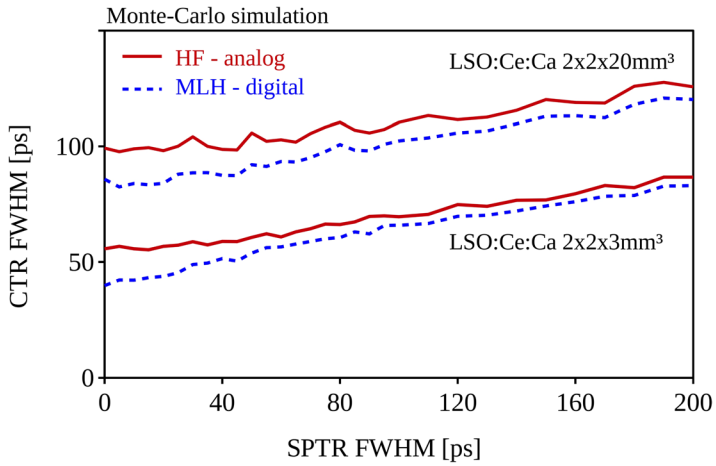

Figure 17. CTR simulated with LSO:Ce:Ca as a function of the SPTR for the analog SiPM with leading edge time estimation or digital SiPM with maximum likelihood (MLH) time estimation. The plot shows complete Monte-Carlo simulations including 7 Cherenkov photons produced in the 390–750 nm range with a weighted PDE of 42% (FBK NUV-HD 40 μm with resin window), whereas the LSO:Ce:Ca emission is detected with a weighted PDE of 59%.

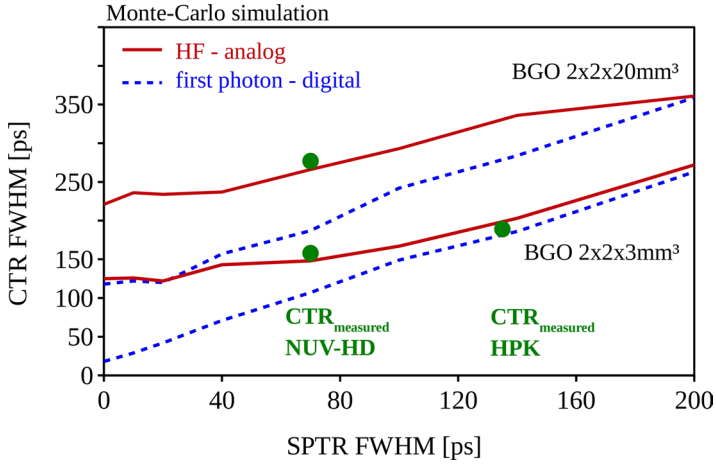

Figure 18. CTR simulated with BGO as a function of the SPTR for the analog SiPM with leading edge time estimation and digital SiPM using only the first photon detected. In the Monte-Carlo simulation we include 17 Cherenkov photons produced in the 310–850 nm range with a PDE of 39.2% (FBK NUV-HD 40 μm), whereas the BGO emission is detected with a weighted PDE of 47.3%.

in equation (1), as we assume an effective rise time of 68 ps. It should be mentioned that CTR measurements with LSO:Ce codoped with 0.4%Ca were performed with a $2 \times 2 \times 3$ mm^3 crystal, where the 2×2 mm^2 face opposite to the SiPM was unpolished leading to a slight gain in LTE (Gundacker 2014). Hence, the CTR performance of the 0.2%Ca crystal (fully polished) is a bit worse than that for the 0.4%Ca crystal. We further want to emphasize that equation (2) does not account for prompt (Cherenkov) emission in the crystal. This could explain the higher CTR of BGO as compared to the prediction of equation (2) (seen in figure 16), because Cherenkov photons dominate the time estimation in BGO. The omission of Cherenkov photons in equation (2) might also explain, at least to some extent, the deviation of the LSO:Ce:Ca results from the predicted value or curve shown in figure 16. The reason is that a mixing of Cherenkov and scintillation photons can lead to a deterioration of the CTR (Gundacker *et al* 2016b), because the scintillation emission is delayed with respect to the prompt Cherenkov radiation. This delay or bias can induce an additional spread in the photostatistics and, hence, worsen the CTR.

To summarize, figure 16 gives an illustration of the intrinsic timing capabilities of the various tested scintillation materials coupled to the best available SiPMs with high PDE and SPTR at this time. In this sense BaF_2 and CsI:undoped appear as interesting candidates for PET applications, together with the well known excellent performance of divalent-ion codoped L(Y)SO:Ce.

6. Prospects of timing with LSO:Ce and BGO in TOF-PET

6.1. Comparing the digital and analog SiPM for LSO:Ce:Ca readout

The analog SiPM with its high-frequency readout, despite its excellent results produced by it in this work, is intrinsically limited in what might be considered as the ultimate time resolution reachable in multi photon counting systems. Limitations arise from bandwidth filtering, electronic noise and the leading edge time estimator, being in fact an average estimator of the first photons detected (Gundacker *et al* 2015). On the other hand, the so-called fully digital SiPM capable to record the time stamp of each photon detected, makes it possible to use the more sophisticated maximum likelihood (MLH) time estimator for ultimate timing precision (Gundacker *et al* 2015). We therefore ran comparative Monte Carlo simulations to investigate these two different types of SiPMs, for which results are shown in figure 17. We observe that the digital approach indeed achieves a better CTR for low SiPM-SPTR values. This improvement is mostly mediated by the presence of prompt photons (Cherenkov), the negligible electronic noise and the absence of bandwidth limitations in the fully digital SiPM.

6.2. The impact of the SPTR to achieve better timing with BGO

In figure 18 we show results from Monte-Carlo simulations of the CTR achievable with BGO of $2 \times 2 \times 3$ mm^3 and $2 \times 2 \times 20$ mm^3 size, when varying the SPTR from 0 ps to 200 ps FWHM. Taking as input the measured 17 Cherenkov photons produced in the 310–850 nm range (see table 5) and the BGO scintillation kinetics (see table 6) we have reached good agreement between measurements and simulation. Using FBK NUV-HD SiPMs with 40 μm SPAD size we measure for the $2 \times 2 \times 3$ mm^3 BGO a CTR of 158 $\pm$ 3 ps FWHM and for the $2 \times 2 \times 20$ mm^3 a CTR of 277 $\pm$ 3 ps FWHM, both in good agreement with our Monte-Carlo simulations outcome of 148 ps and 266 ps FWHM, respectively (figure 18). In the simulations we included the measured intrinsic SPTR of 70 ps FWHM and a weighted PDE of 39.2% for the Cherenkov emission and 47.3% for the BGO emission. For the digital SiPM simulations in figure 18 we only use the first detected photon to estimate the 511 keV gamma conversion time. We furthermore tested another more sophisticated maximum likelihood estimation algorithm and found the simpler first photon time estimator sufficient and easier to implement in a real detector system. As seen in figure 18, the CTR achievable with BGO can indeed benefit from improving the SPTR of the SiPM, whereas the digital (first photon) approach has a clear advantage at very low SPTR values only. It should also be mentioned that the exact value of the CTR achievable with BGO, in the case of very low SPTR values, is strongly dependent on the number of Cherenkov photons detected. Furthermore, we did not include optical crosstalk in the SiPM in our simulations. This will be investigated in future studies.

In figure 18 we additionally show the measured CTR of 189 $\pm$ 5 ps FWHM when coupling the $2 \times 2 \times 3$ mm^3 BGO crystal to the HPK S13360 SiPM with 50 μm SPAD size. The main reason for the observed worse CTR with the HPK S13360 SiPM, as compared to the NUV-HD SiPM, is the inferior intrinsic SPTR (135 ps FWHM) of the HPK device, being almost twice as high as that of the NUV-HD SiPM. On the other hand, the weighted PDE of the HPK SiPM for BGO Cherenkov emission in the range of 310–850 nm is 44.9% and, hence, slightly better than that of the FBK SiPM (39.2%). This is due to the higher PDE of the HPK SiPM at larger wavelengths ($\sim$500 nm), and to some extent explains why the measured CTRs with HPK-SiPMs are slightly better than the predicted MC values; bearing in mind that the MC simulations are adapted to FBK-SiPMs.

7. Conclusion

We have made an evaluation of the single photon timing performance of the best state-of-the-art SiPMs available on the market and of those produced in reputed research institutes. We found that the intrinsic SPTR of modern analog-SiPMs can reach 70 ps FWHM when illuminating the whole device, as in the case of FBK NUV-HD with 4×4 mm^2 active area and 40 μm SPAD size. This measurement was achieved with high-frequency front-end electronics. HPK SiPMs do perform a little worse, with intrinsic SPTR values of 117 ps FWHM for the S14160, 3×3 mm^2 device with 50 μm SPAD size, although having a higher PDE in the green than FBK. Furthermore, we showed that the CTR with the high-frequency readout strongly correlates with the measured SPTR, ultimately achieving an unprecedented CTR of 58 ps FWHM with $2 \times 2 \times 3$ mm^3 LSO:Ce crystals codoped with 0.4%Ca and read out by FBK NUV-HDs. Improvements in the SPTR lead to noticeable CTR gains for TOF-PET applications, when L(Y)SO:Ce(:Ca) crystals are being used.

The high-frequency readout electronics, the high PDE in the near ultraviolet and the high SPTR of modern SiPMs lead to an excellent achievable timing with BGO. We measured a CTR of 158 ps FWHM for $2 \times 2 \times 3$ mm^3 and 277 ps FWHM for $2 \times 2 \times 20$ mm^3 crystals coupled to FBK NUV-HD SiPMs. These values stay almost the same when increasing the crystal cross section, i.e. for example we measured a CTR of 167 ps FWHM for $3 \times 3 \times 3$ mm^3 and 235 ps FWHM for $3 \times 3 \times 15$ mm^3 BGO crystals. To further investigate the limits in achievable timing with BGO we measured the average number of prompt (Cherenkov) photons produced in BGO to be 17 $\pm$ 3 upon 511 keV interaction, via a time correlated single photon counting setup. This

value is very close to our Geant4 based estimation of 18.8 Cherenkov photons generated. Thorough Monte-Carlo simulations have further shown that the digital SiPM readout, using only the first photon detected, would greatly benefit from SPTR values as low as 10 ps FWHM in order to improve the CTR with BGO. In this sense, CTR values of ∼30 ps FWHM seem to be possible with $2 \times 2 \times 3$ mm^3 and ∼122 ps FWHM with $2 \times 2 \times 20$ mm^3 BGO crystals. However, there are still other conceivable strategies of reading the photons from the crystal that have the potential to improve these figures for high-precision TOF-PET systems, e.g. reading the light with digital SiPMs on all sides of a block detector.

We have tested a large amount of scintillating materials and can conclude that the measured CTR values can be sorted and even predicted by a simple analytic CTR equation, using only the scintillation kinetics, light yield, LTE and photon time spread of the crystals together with SiPM parameters like the PDE and SPTR. Amidst the vast amount of tested scintillators we found that BC422 plastic scintillators give extraordinarily good timing, achieving a CTR of 35 ps FWHM with only 340 keV energy deposited in the scintillator. Due to the low density of the plastic, this scintillator as such is of lower interest for PET, but neverthelss could be used as a fast time tagger in a metamaterial (hybrid scintillator) approach or for lower gamma energies, as well as in applications where sensitivity plays a secondary role. An interesting candidate for ultrafast timing remains cross-luminescence in BaF_2, emitted around 200 nm, accessible by the appearance of SiPMs with a PDE of ∼22% in the deep-UV. With VUV-HD SiPMs from FBK, developed for dark-matter search, we measured CTR values of 51 ± 5 ps FWHM, which still leaves room for large improvements by pushing the PDE to values of modern standard SiPMs.

We have shown that with state-of-the-art SiPMs and 20mm long LSO:Ce:Ca crystals, TOF-PET with a CTR of 100 ps FWHM is possible, without sacrificing on sensitivity, nor increasing the number of readout channels. Considering cost effectiveness and the integration in a PET system with the goal of delivering a high sensitivity or 511 keV gamma detection efficiency, it nevertheless becomes clear that today's common scintillation materials will not allow to significantly overcome the 100 ps barrier. Hence, other ways of intelligent crystal readout or novel scintillation mechanisms have to be investigated, e.g. digital high-performance SiPM readout of the crystal, employing depth of interaction correction, collecting more of the produced light in the crystal, or ultrafast scintillation emission in quantum confined systems like CdSe nanoplatelets integrated in a metamaterial approach.

Acknowledgments

This work has been performed in the framework of the Crystal Clear Collaboration and the TICAL ERC Grant #38953. The authors would like to express their highest gratitude to Joshua W Cates and Sergey Vinogradov for many interesting and fruitful discussions. Further we would like to thank Dominique Deyrail for thoroughly cutting and polishing several crystal samples used in this work, Sergey Omelkov for providing CsI:undoped, A Petrosyan for providing the LuAG type samples and Prof A Yoshikawa and C&A for providing GAGG:Ce:Mg and GFAG samples. We want to thank FBK (Alberto Gola, Massimo Capasso, Giovanni Paternoster), Ketek (Thomas Ganka, Florian Schneider), Broadcom (Stefan Brunner), SensL (Carl Jackson) and HPK (Marius Metzger) for kindly providing SiPM samples used in this study. Last but not least we want to express our sincere thanks to Tom Meyer for thoroughly proofreading this manuscript.

ORCID iDs

Stefan Gundacker https://orcid.org/0000-0003-2087-3266
Rosana Martinez Turtos https://orcid.org/0000-0002-1077-4849

References

Acerbi F and Gundacker S 2019 Understanding and simulating SiPMs *Nucl. Instrum. Methods Phys. Res.* A **926** 16–35
Bollinger L and Thomas G 1961 Measurement of the time dependence of sintillation intensity by a delayed-coincidence method *Rev. Sic. Instrum.* **32** 1044–50
Brunner S and Schaart D R 2017 BGO as a hybrid scintillator/Cherenkov radiator for cost-effective time-of-flight PET *Phys. Med. Biol.* **62** 4421–39
Cates J W and Levin C S 2019 Electronics method to advance the coincidence time resolution with bismuth germanate *Phys. Med. Biol.* **64** 175016
Cates J W, Gundacker S, Auffray E, Lecoq P and Levin C S 2018 Improved single photon time resolution for analog SiPMs with front end readout that reduces influence of electronic noise *Phys. Med. Biol.* **63** 185022
Cherenkov P 1934 Visible emission of clean liquids by action of γ radiation *Dokl. Akad. Nauk SSSR* **451**
Conti M and Bendriem B 2019 The new opportunities for high time resolution clinical TOF PET *Clin. Transl. Imaging* **7** 139–47
Eckert P, Schultz-Coulon H, Shen W, Stamen R and Tadday A 2010 Characterisation studies of silicon photomultipliers *Nucl. Instrum. Methods Phys. Res.* A **620** 217–26
Garutti E and Musienko Y 2019 Radiation damage of SiPMs *Nucl. Instrum. Methods Phys. Res.* A **926** 69–84
Gola A, Acerbi F, Capasso M, Marcante M, Mazzi A, Paternoster G, Piemonte C, Regazzoni V and Zorzi N 2019 Nuv-sensitive silicon photomultiplier technologies developed at Fondazione Bruno Kessler *Sensors* **19** 308

Gundacker S 2014 Time resolution in scintillator based detectors for positron emission tomography *PhD Thesis* Vienna University of Technology

Gundacker S, Acerbi F, Auffray E, Gola A, Nemallapudi M, Paternoster G, Piemonte C and Lecoq P 2016a State of the art timing in TOF-PET detectors with LuAG, GAGG and L(Y)SO scintillators of various sizes coupled to FBK-SiPMs *J. Instrum.* **11** P08008

Gundacker S, Auffray E, Frisch B, Jarron P, Knapitsch A, Meyer T, Pizzichemi M and Lecoq P 2013 Time of flight positron emission tomography towards 100 ps resolution with L(Y)SO: an experimental and theoretical analysis *J. Instrum.* **8** P07014

Gundacker S, Auffray E, Jarron P, Meyer T and Lecoq P 2015 On the comparison of analog and digital SiPM readout in terms of expected timing performance *Nucl. Instrum. Methods Phys. Res.* A **787** 6–11

Gundacker S, Auffray E, Pauwels K and Lecoq P 2016b Measurement of intrinsic rise times for various L(Y)SO and LuAG scintillators with a general study of prompt photons to achieve 10 ps in TOF-PET *IOP Phys. Med. Biol.* **61** 2802–37

Gundacker S, Knapitsch A, Auffray E, Jarron P, Meyer T and Lecoq P 2014 Time resolution deterioration with increasing crystal length in a TOF-PET system *Nucl. Instrum. Methods Phys. Res.* A **737** 92–100

Gundacker S, Turtos R M, Auffray E and Lecoq P 2018 Precise rise and decay time measurments of inorganic scintillators by means of x-ray and 511 keV excitation *Nucl. Instrum. Methods Phys. Res.* A **891** 42–52

Gundacker S, Turtos R M, Auffray E, Paganoni M and Lecoq P 2019 High-frequency SiPM readout advances measured coincidence time resolution limits in TOF-PET *Phys. Med. Biol.* **64** 9

Knapitsch A 2012 Photonic crystals: enhancing the light output of scintillation based detectors *PhD Thesis* Vienna University of Technology

Kwon S, Gola A, Ferri A, Piemonte C and Cherry S 2016 Bismuth germanate coupled to near ultraviolet silicon photomultipliers for time-of-flight PET *Phys. Med. Biol.* **61** L38–47

Laval M, Moszyński M, Allemand R, Cormoreche E, Guinet P, Odru R and Vacher J 1983 Barium fluoride—inorganic scintillator for subnanosecond timing *Nucl. Instrum. Methods Phys. Res.* **206** 169–76

Lecoq P 2017 Pushing the limits in time-of-flight PET imaging *IEEE Trans. Radiat. Plasma Med. Sci.* **1** 476–85

Lecoq P, Annenkov A, Gektin A, Korzhik M and Pedrini C 2006 *Inorganic Scintillators for Detector Systems. Physical Principles and Crystal Engineering* (Berlin: Springer)

Moskal P *et al* 2019 Feasibility study of the positronium imaging with the j-PET tomograph *Phys. Med. Biol.* **64** 055017

Fishburn M W and Charbon E 2010 System tradeoffs in gamma-ray detection utilizing SPAD arrays and scintillator *IEEE Trans. Nucl. Sci.* **57**

Nemallapudi M, Gundacker S, Lecoq P and Auffray E 2016 Single photon time resolution of state of the art SiPMs *J. Instrum.* **11** P10016

Omelkov S, Nagirnyi V, Gundacker S, Spassky D A, Auffray E, Lecoq P and Kirm M 2018 Scintillation yield of hot intraband luminescence *J. Lumin.* **198** 260–71

Piemonte C, Acerbi F, Ferri A, Gola A, Paternoster G, Regazzoni V, Zappala G and Zorzi N 2016 Performance of NUV-HD silicon photomultiplier technology *IEEE Trans. Electron. Dev.* **63** 1111–6

Seifert S, Steenbergen J, van Dam H and Shaart D 2012 Accurate measurement of the rise and decay times of fast scintillators with solid state photon counters *J. Instrum.* **7** P09004

Turtos R M, Gundacker S, Auffray E and Lecoq P 2019a Towards a metamaterial approach for fast timing in PET: experimental proof-of-concept *Phys. Med. Biol.* **64** 185018

Turtos R M *et al* 2019b On the use of CdSe scintillating nanoplatelets as time taggers for high-energy gamma detection *npj 2D Mater. Appl.* **3** 37

van der Laan D J J, Schaart D R, Maas M C, Beekman F J, Bruyndonckx P and van Eijk C W E 2010 Optical simulation of monolithic scintillator detectors using GATE/GEANT4 *Phys. Med. Biol.* **55** 1659–75

Vinogradov S 2018 Approximations of coincidence time resolution models of scintillator detectors with leading edge discrimination *Nucl. Instrum. Methods Phys. Res.* A **912** 149–53

Williams P A, Rose A H, Lee K S, Conrad D C, Day G W and Hale P D 1996 Optical, thermo-optic, electro-optic, and photoelastic properties of bismuth germanate (Bi4Ge3O12) *Appl. Opt.* **35** 3562–9